International Journal of Engineering & Applied Sciences (IJEAS)
Vol.15, Issue 4 (2023) 163-183
http://dx.doi.org/10.24107/ijeas.1386832
Int J Eng Appl Sci 15(4) (2023) 163-183

Large Deformation Analysis of Hyperelastic Continuum with Hexahedral Adaptive Finite Elements

Mustafa Tekin [a], Bahadır Alyavuz [b]*

[a] *Gazi University, Graduate School of Natural and Applied Sciences, Department of Civil Engineering, Ankara, Türkiye*
[b] *Gazi University, Faculty of Engineering, Department of Civil Engineering, Ankara, Türkiye*

✉: mustafatekincsb@gmail.com[a], balyavuz@gazi.edu.tr[b] : 0000-0003-2130-6407[a],0000-0003-4643-4368[b]

Received:06.10.2023, Revised: 12.12.2023, Accepted: 23.12.2023

Abstract

The use of hyperelastic materials capable of large deformations, such as elastomeric bearings used to reduce seismic effects, is quite common in civil engineering. Such environments are, in most cases, addressed by numerical solution techniques such as the finite element method. In case of large deformations, nonlinear analysis is used in the solution. In the study presented here, large deformations of a hyperelastic continuum expressed by the Mooney-Rivlin material model are calculated using hexahedral adaptive finite elements. A code was written in MATLAB using the total Lagrangian formulation for the nonlinear adaptive finite element solution. Comparisons were made with Abaqus software to check the consistency of the results obtained from this program. It has been observed that local refinements in the adaptive element mesh occur in the regions where they are needed. Considering the variation of maximum displacement and maximum stress with the number of elements, it has been observed that mesh refinement creates a convergent solution.

Keywords: Hyperelasticity, adaptive finite element method, hexahedral elements.

1. Introduction

Hyperelasticity is used for materials that are nonlinear and capable of large deformation, where the constitutive equation is derived from an elastic potential. These types of materials are frequently encountered in the field of civil engineering as well as in various sectors. One of the important area of use is elastomeric bearings used for reducing seismic forces on structures. These environments, which involve large deformation of hyperelastic materials, are in most cases handled with numerical solution techniques such as finite element method (FEM).

Regarding the solutions obtained from FEM, how the problem geometry is divided into finite elements is an important factor affecting the solution. Results generally become more accurate as the finite element size decreases. The process of dividing the elements into smaller elements is referred as mesh refinement. As a result of mesh refinement, the solution time increases as the number of elements increases. Therefore, an effective solution can be achieved by refining the mesh only where necessary. At this point, mesh refinement can be done in user-defined regions, or an automatical mesh refinement strategy based on a particular predefined refinement criterion can be used. The second one can be called adaptive mesh refinement. The method turns into adaptive finite element analysis with a criterion that uses the results obtained from finite element analysis.

In modeling a three-dimensional geometry, tetrahedral elements (tetrahedrons), which consist of four triangular faces, and hexahedral elements (hexahedrons), which consist of six faces, are commonly used. Tetrahedrons enable the creation of an element mesh that better represents

geometry boundaries and enables easier transition from small elements to large elements, especially for non-uniform geometries and adaptive solutions. On the other hand, using hexahedrons shortens the calculation time by requiring fewer elements and provides more accurate solutions due to the additional terms in the shape functions used for interpolation [1]. Linear tetrahedral elements also exhibit "volumetric locking" and "shear locking" problems due to their more rigid behavior, so hexahedral finite elements are preferred [2].

Creating a finite element mesh using hexahedral elements can be done by several different methods. The element mesh created by dividing the geometry into uniformly distributed hexahedral elements is called a regular element mesh. The problem geometry is divided into finite elements using a grid with equal number of points on opposite edges [3]. A regular element mesh is a fast option in cases where there are no curvilinear boundaries. Using an unequal number of points on opposite edges makes the distribution of hexahedral elements irregular. Irregular finite element mesh, which provides a more flexible option in dividing the geometry into elements, is an element mesh that must be created in complex geometries with curvilinear surfaces. This type of finite element mesh can be created by direct and indirect methods. Dividing [4] or combining [5] tetrahedron elements created as the initial element mesh is an indirect method for creating hexahedral elements. With grid-based methods, which are direct methods, a regular hexahedral grid is first placed in the geometry, and then the gaps between the grid and the geometry boundary are filled with hexahedral elements [3]. Direct and indirect methods such as sweeping [6,7], advancing front [1, 8], and subdivision [9] are other methods that can be used to create hexahedral element meshes in complex geometries.

In a mesh containing hexahedral elements, dividing an element into smaller elements to achieve regional refinement is a frequently used method. However, a discontinuity occurs between the divided element and neighboring elements. Therefore, neighboring elements must be divided in addition to the divided element to ensure continuity. These elements, which provide continuity in the hexahedral element mesh refinement, are defined as transition elements [10]. Hexahedron partitioning types and shapes of transition elements for different local refinement strategies have been shown in various studies [10-12].

The adaptive element mesh can be created using geometric features of the problem or using a calculated indicator [13]. In geometric adaptive methods, refinement is done through points, edges, and surfaces on the element depending on the characteristics of the problem geometry [14]. Geometric features such as surface curvatures, sharp-edged regions, and boundaries, can be used to create a geometric adaptive element mesh [14-19]. In methods based on an indicator, an error estimator is calculated at each element using the initial mesh [20-24]. Refinement or coarsening is made in the elements to create an evenly distributed error estimate in the mesh. Variation of parameters such as stress, strain, or temperature obtained from an initial FEM solution can also be used to create an adaptive finite element mesh [25, 26].

Although the finite element method was initially created to solve linear behavior, it was expanded over time to model the nonlinear behavior of hyperelastic materials, including compressibility [27-29] and incompressibility [30-32]. In related studies, triangular elements [33] and quadrilateral elements [34, 35] for two dimensional problems, tetrahedral elements [36] and hexahedral [31,32,37,38,39] elements in three-dimensional problems were frequently used. In order to obtain more realistic results and quick solutions for hyperelastic continua, 2d triangular adaptive finite elements [40-42], 2d quadrilateral adaptive elements [35], 2d quadtree adaptive finite elements [43], 3d octree adaptive finite elements [44], and 3d tetrahedral adaptive finite elements [40,45] were used.
In this study, large deformations of a hyperelastic medium were calculated with three-dimensional hexahedral adaptive finite elements. A program was written in the MATLAB

environment using the total Lagrangian formulation. The results were examined by comparing them with Abaqus [46] software.

2. Theory and Formulation

2.1 Kinematics and Constitutive Theory

We consider the continuum shown in Fig. 1 to study the nonlinear motion of a nearly incompressible hyperelastic body. A continuous medium is shown that moves from the reference configuration, that is, the undeformed state, to the spatial configuration, that is, the deformed state, due to the forces and/or displacements acting on it. In subsequent calculations, scalar quantities are expressed in italics, and vector and tensor quantities are expressed in bold letters. Additionally, the elements of any vector or tensor are shown with index notation. Capital letters will be used in square brackets for matrices representing the elements of tensor quantities.

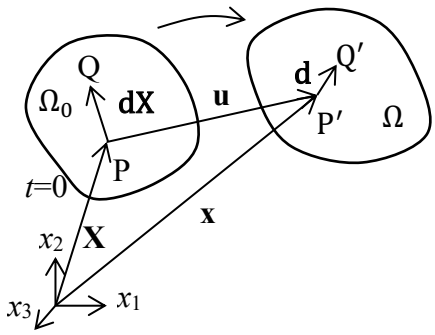

Fig. 1. Reference (Ω_0) and spatial configuration (Ω) of the continuous medium

The deformation gradient tensor is important for calculations involving large deformations in continuum mechanics. As seen in Eq. (1), the deformation gradient tensor **F** is the tensor that transforms an infinitesimal **dX** vector defined in the reference configuration into the **dx** vector in the spatial configuration. It is defined as the derivative of the spatial position vector with respect to the reference position vector.

$$\mathbf{dx}=\mathbf{F}\mathbf{dX} \quad \text{veya} \quad F_{ij}=\frac{\partial x_i}{\partial X_j} \tag{1}$$

The strain energy function expressed in unit volume is used in the stress calculation for a hyperelastic continuum. For an isotropic medium, this quantity is expressed with the help of principal invariants in most cases. The principal invariants to be used here are the principal invariants of the Right Cauchy - Green deformation tensor **C** given by Eq. (2).

$$\mathbf{C}=\mathbf{F}^{\mathrm{T}}\mathbf{F} \tag{2}$$

The principal invariants of the right Cauchy - Green deformation tensor are written in terms of the eigenvalues of this tensor, as follows.

$$I_1=\mathrm{tr}(\mathbf{C})=\lambda_1^2+\lambda_2^2+\lambda_3^2\,,\; I_2=\frac{1}{2}\left[(\mathrm{tr}\mathbf{C})^2-\mathrm{tr}(\mathbf{C}^2)\right]=\lambda_1^2\lambda_2^2+\lambda_2^2\lambda_3^2+\lambda_3^2\lambda_1^2\,,\; I_3=\det(\mathbf{C})=\lambda_1^2\lambda_2^2\lambda_3^2 \tag{3}$$

Here, λ_1^2, λ_2^2 and λ_3^2 represent the eigenvalues of the symmetric right Cauchy – Green deformation tensor, I_1 and I_2 represent the principal invariants related to distortion, and I_3 represent the

principal invariant related to volumetric deformation. A general form of the strain energy function required for stress calculation is given in Eq. (4) [47].

$$W(I_1, I_2, I_3) = \sum_{m+n+k=1}^{\infty} C_{mnk}(I_1-3)^m(I_2-3)^n(I_3-1)^k \quad (4)$$

In this equation, C_{mnk} are the material coefficients. The strain energy function, which can be written by separating the distortional strain resulting from shear stresses and the volumetric strain resulting from normal stresses, is possible by using the following constants [47].

$$J_1=I_1I_3^{1/3},\ J_2=I_2I_3^{2/3},\ J_3=I_3^{1/2} \quad (5)$$

Here, the values J_1, J_2 and J_3 are reduced invariants.

Rubber-type materials used in engineering are called "nearly incompressible" because they can be compressed to a very low amount. The Mooney-Rivlin material model is often used when calculating the strain energy function of these hyperelastic materials because of its simple definition. Despite its difficulties representing the hardening of the material, it is a good model for large strains up to 100% strain [47]. There are four different types depending on the number of material constants used in the model. These are material models with 2, 3, 5 and 9 constants. For this model, the strain energy function is calculated with Eq. (6) using the reduced invariants given in Eq. (5). In this Equation, W_1 refers to the distortion energy function and W_2 refers to the energy function resulting from volumetric change.

$$W(J_1, J_2, J_3) = W_1(J_1, J_2)+W_2(J_3) = C_{10}(J_1-3)+C_{01}(J_2-3)+\frac{K}{2}(J_3-1)^2 \quad (6)$$

Here C_{10}, C_{01} are material constants and K is the bulk modulus. For a completely incompressible material, the bulk modulus should theoretically be infinite. For nearly incompressible medium, the solution using a large K value is referred to as the penalty method and K as the penalty parameter. In case of three-dimensional small unit strain, the value $2(C_{10}+C_{01})$ corresponds to the shear modulus of the material, and the value $6(C_{10}+C_{01})$ corresponds to the elasticity modulus of the material. Theoretically, for incompressible materials the Poisson's ratio should be 0,5, but for nearly incompressible behavior the Poisson's ratio is between 0,49 and 0,5.

The second Piola – Kirchhoff stress **S** is obtained by the derivative of the strain energy function, W, with respect to the Lagrange strain tensor, **E**, for the constitutive equations representing the relation between stress and strain, as follows,

$$\mathbf{S}=\frac{\partial W}{\partial \mathbf{E}}=\frac{\partial W_1}{\partial J_1}\frac{\partial J_1}{\partial \mathbf{E}}+\frac{\partial W_1}{\partial J_2}\frac{\partial J_2}{\partial \mathbf{E}}+\frac{\partial W_2}{\partial J_3}\frac{\partial J_3}{\partial \mathbf{E}} \quad (7)$$

The derivative of the second Piola – Kirchhoff stress with respect to the Lagrange strain tensor is equal to the fourth order constitutive tensor, **D**.

$$\mathbf{D}=\frac{\partial \mathbf{S}}{\partial \mathbf{E}} \quad (8)$$

By calculating the tensor **D** in terms of material constants, the relationship between stress and strain is established.

2.2 Nonlinear Finite Element Formulation

In the total Lagrangian formulation, the reference configuration of the continuum shown in Fig. 1 is used [48]. In addition, the frame of reference in this configuration is considered to be fixed. Independent variables are (**X**, *t*) for position and time, and the displacement dependent variable is **u**(**X**, *t*).

The "approximate displacement function" is expressed in terms of the shape functions written in the reference position and the displacements at the nodes as given in Eq. (9). Additionally, the displacement gradient and the Lagrange strain tensor are also written in terms of this "approximate displacement function" using spatial derivatives.

$$
\begin{aligned}
u_1 &= \sum_{j=1}^{8} d_{1j}N_j = d_{11}N_1 + d_{12}N_2 + d_{13}N_3 + \cdots + d_{18}N_8 \\
u_2 &= \sum_{j=1}^{8} d_{2j}N_j = d_{21}N_1 + d_{22}N_2 + d_{23}N_3 + \cdots + d_{28}N_8 \\
u_3 &= \sum_{j=1}^{8} d_{3j}N_j = d_{31}N_1 + d_{32}N_2 + d_{33}N_3 + \cdots + d_{38}N_8
\end{aligned} \tag{9}
$$

According to the principle of minimum potential energy, the potential energy of the elastic system is equal to the difference between the stored strain energy Π_{int} in the system and the work done by external forces Π_{ext}. For an approximate solution in nonlinear finite element analysis, an iterative solution is made based on the principle of approximating this difference to the smallest value.

The strain energy stored in the system is calculated by integrating the strain energy density over the undeformed entire volume. The work done by the forces is calculated by the integral of the product of the body forces with the displacement of the nodes over the entire volume and the integral of the displacement of the nodes at the boundaries of the continuum multiplied by the external forces on the boundaries. Potential energy of the system can be written as follows.

$$
\Pi=\Pi_{ext}-\Pi_{int}= \iiint_{\Omega_0} W(\mathbf{E})d\Omega - \iiint_{\Omega_0} \mathbf{u}^T\mathbf{f}_b d\Omega - \iint_{\tau_0} \mathbf{u}^T\mathbf{t}\, d\tau \tag{10}
$$

If the displacement field **u** is perturbed by $\bar{\mathbf{u}}$ in an arbitrary direction and magnitude, equating the variation of potential energy $\bar{\Pi}$ to zero yields the following variational equation.

$$
\bar{\Pi}= \iiint_{\Omega_0} \frac{\partial W(\mathbf{E})}{\partial \mathbf{E}} : \bar{\mathbf{E}}\, d\Omega - \iiint_{\Omega_0} \bar{\mathbf{u}}^T\mathbf{f}_b d\Omega - \iint_{\tau_0} \bar{\mathbf{u}}^T\mathbf{t}\, d\tau = 0 \tag{11}
$$

The displacement-strain transformation matrix [**B**] relates nodal displacements to strain. In linear analysis, it only includes spatial derivatives of shape functions. It also includes the deformation gradient tensor for the nonlinear analysis. While it is constant in linear analysis, in nonlinear analysis it changes with respect to displacement because of the deformation gradient tensor.

Linear displacement-strain transformation matrix [$\mathbf{B}_L$],

$$[\mathbf{B}_L]=\begin{bmatrix} N_{1,1} & 0 & 0 & N_{2,1} & \dots & 0 & 0 \\ N_{1,2} & 0 & 0 & N_{2,2} & \dots & 0 & 0 \\ N_{1,3} & 0 & 0 & N_{2,3} & \dots & 0 & 0 \\ 0 & N_{1,1} & 0 & 0 & \dots & N_{8,1} & 0 \\ 0 & N_{1,2} & 0 & 0 & \dots & N_{8,2} & 0 \\ 0 & N_{1,3} & 0 & 0 & \dots & N_{8,3} & 0 \\ 0 & 0 & N_{1,1} & 0 & \dots & 0 & N_{8,1} \\ 0 & 0 & N_{1,2} & 0 & \dots & 0 & N_{8,2} \\ 0 & 0 & N_{1,3} & 0 & \dots & 0 & N_{8,3} \end{bmatrix} \tag{12}$$

and $[\mathbf{B}_N]$ transformation matrix for nonlinear analysis is given by the following equation [47].

$$[\mathbf{B}_N]=\begin{bmatrix} F_{11}N_{1,1} & F_{21}N_{1,1} & F_{31}N_{1,1} & \dots & F_{31}N_{8,1} \\ F_{12}N_{1,2} & F_{22}N_{1,2} & F_{32}N_{1,2} & \dots & F_{32}N_{8,2} \\ F_{13}N_{1,3} & F_{23}N_{1,3} & F_{33}N_{1,3} & \dots & F_{33}N_{8,3} \\ F_{12}N_{1,1}+F_{11}N_{1,2} & F_{22}N_{1,1}+F_{21}N_{1,2} & F_{32}N_{1,1}+F_{31}N_{1,2} & \dots & F_{32}N_{8,1}+F_{31}N_{8,2} \\ F_{13}N_{1,2}+F_{12}N_{1,3} & F_{23}N_{1,2}+F_{22}N_{1,3} & F_{33}N_{1,2}+F_{32}N_{1,3} & \dots & F_{33}N_{8,2}+F_{32}N_{8,3} \\ F_{13}N_{1,1}+F_{11}N_{1,3} & F_{23}N_{1,1}+F_{21}N_{1,3} & F_{33}N_{1,1}+F_{31}N_{3,1} & \dots & F_{33}N_{8,1}+F_{31}N_{8,3} \end{bmatrix} \tag{13}$$

Here, N_I denotes the shape function and $N_{I,j}$ denotes the derivative of the shape function with respect to position, and F_{ij} denotes the corresponding element of the deformation gradient.

Due to the nonlinearity in the displacement-strain relationship, there is no easy direct solution to the variational equations. It is possible to obtain the solution by the iterative Newton-Raphson method in combination with a series of successive linearizations.

Since internal forces are a nonlinear function of the deformation, the resulting force-displacement equation will need to be solved iteratively. A general nonlinear equation can be solved by the Newton-Raphson method along with a series of linearization operations. An iterative method such as the Newton-Raphson method requires the use of a tangent stiffness matrix. In the total Lagrangian formulation, the tangent stiffness matrix corresponds to the discretization of the linearized energy form. The 9x9 size [Σ] matrix, which will be used to obtain the linear part of the tangent stiffness matrix, is obtained with Eq. (14).

$$\bar{\mathbf{S}}=\begin{bmatrix} S_{11} & S_{12} & S_{13} \\ S_{21} & S_{22} & S_{23} \\ S_{31} & S_{32} & S_{33} \end{bmatrix},\ \bar{\mathbf{0}}=\begin{bmatrix} 0 & 0 & 0 \\ 0 & 0 & 0 \\ 0 & 0 & 0 \end{bmatrix},\ [\Sigma]=\begin{bmatrix} \bar{\mathbf{S}} & \bar{\mathbf{0}} & \bar{\mathbf{0}} \\ \bar{\mathbf{0}} & \bar{\mathbf{S}} & \bar{\mathbf{0}} \\ \bar{\mathbf{0}} & \bar{\mathbf{0}} & \bar{\mathbf{S}} \end{bmatrix} \tag{14}$$

Here **S** is the second Piola-Krichhoff stress tensor. Tangent stiffness matrix $[\mathbf{K}_T]$, can be written by adding linear and non-linear parts as,

$$[\mathbf{K}_T] = \iiint_{\Omega_0}\left([\mathbf{B}_N]^T[\mathbf{D}][\mathbf{B}_N]+[\mathbf{B}_L]^T[\textstyle\sum][\mathbf{B}_L]\right)\mathrm{d}\Omega \tag{15}$$

Generally, the integral in above equation is obtained by Gauss quadrature. 2x2x2 integration points were used for the hexahedral element.

Internal forces $\mathbf{f}^{int}$ are obtained by the following discrete version of the energy form [47].

$$a(\mathbf{u},\bar{\mathbf{u}})= \iiint_{0_\Omega} \mathbf{S}:\bar{\mathbf{E}}\, d\Omega= \{\bar{\mathbf{d}}\}^T \iiint_{0_\Omega} [\mathbf{B}_N]^T \{\mathbf{S}\} d\Omega \equiv \{\bar{\mathbf{d}}\}^T \{\mathbf{f}^{int}\} \quad (16)$$

Using the minimum potential energy principle, the incremental finite element matrix equation is written as follows [47].

$$\{\bar{\mathbf{d}}\}^T [\mathbf{K}_T] \{\Delta\mathbf{d}\} = \{\bar{\mathbf{d}}\}^T \{\mathbf{f}^{ext}-\mathbf{f}^{int}\} \quad (17)$$

Here, $\bar{\mathbf{d}}$ refers to the variation of nodal displacements, $\Delta\mathbf{d}$ refers to the displacement increment, $\mathbf{f}^{ext}$ refers to external forces, $\mathbf{f}^{\text{int}}$ refers to internal forces. By making an initial assumption for node displacements, the increment in displacements, $\Delta\mathbf{d}$, is calculated from the solution of this system of equations and added to the existing node displacements to obtain the new displacement value of the nodes. Thus, one iteration is completed. Iterations continue until the difference between the external forces and internal forces on the right side of the equation approaches zero within a certain tolerance value.

2.3 Adaptive finite element mesh

Refinement of the finite element mesh is often done by the engineer performing the analysis. In the adaptive finite element mesh, refinement is done automatically according to a criterion determined independently of the person. The adaptive finite element mesh can be made in four different ways [49]. With the h-adaptive distribution, the size of the elements is changed; with the p-adaptive distribution, the degree of the element is changed; with the r-adaptive distribution, smaller finite elements are created in the targeted region by moving the mesh, provided that the degree and number of the elements are kept constant. The hp-adaptive distribution uses h- and p-methods together [49,50].

In this study, the h-adaptive method was used with hexahedral finite elements. In order to create the adaptive mesh, the minimum/maximum error indicator was used. The effective stress is the parameter of the minimum/maximum error indicator. In the minimum/maximum error distribution, the average parameter value of the finite elements is first found. The effective stress of all finite elements are compared with this value. If the element's effective stress is more or less than the average at a default value, the element is decided to be divided for the adaptive distribution.

The most commonly used method for mesh refinement is to divide an element into smaller elements. After this division process, the nodes formed in the finite element mesh should be connected to the nodes of another element, and the element edges or surfaces should not be formed in a way that cuts the edges and surfaces of other elements. The element types that can be used for division to achieve this are shown in Fig. 2. Here, an element that has not been divided will be named as a 0-element, and the divided element will be named according to the number of elements formed in it. The elements connecting the divided element to the mesh will be referred to as transition elements.

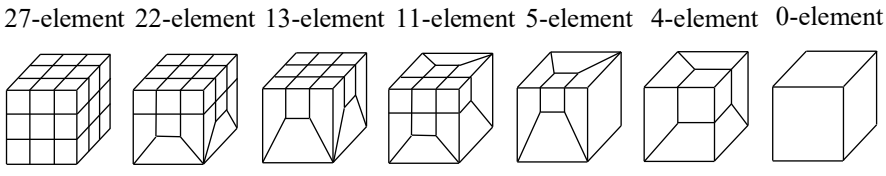

Fig. 2. Types of elements used in the refinement

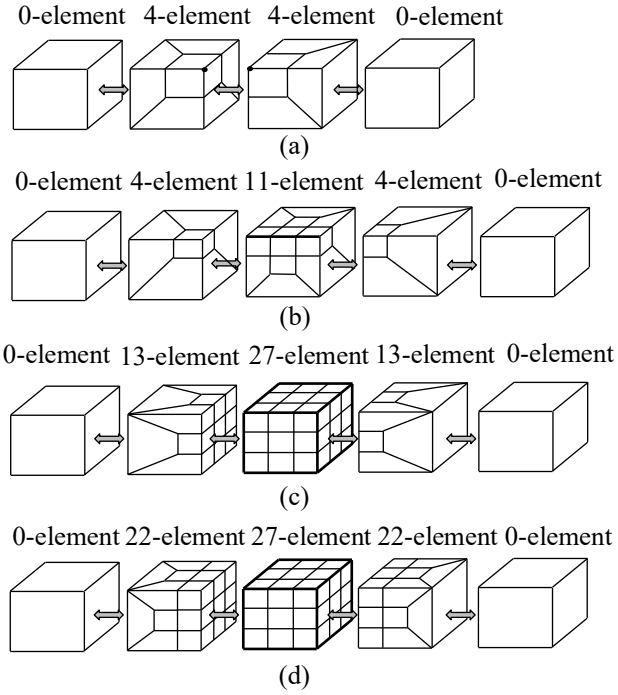

Fig. 3. Refinement strategies a) at a point, b) at an edge, c) and d) at an element

In the refinement, a new finite element mesh can be created using a node, element edge, and element surface or the element itself. If the refinement is decided to be done at a node as shown in Fig. 3a, the element is divided using a 4-element with the transition elements to connect the mesh. Fig. 4 shows a mesh refinement using a node of the mesh. If it is decided to refine the mesh by dividing the whole element, 27-element can be used with the transition elements as shown in Fig. 3c and 3d. The element types that can be connected to the divided element are expressed in Table 1. Additionally, new elements formed in a divided element are shown in Fig. 5.

Table 1. Elements that can be connected to a divided element

Divided element	Transition element
27	27, 22, 13
22	27, 22, 13, 11, 0
13	27, 22, 13, 5, 0
11	22, 11, 4, 0
5	13, 5, 0
4	11, 4, 0

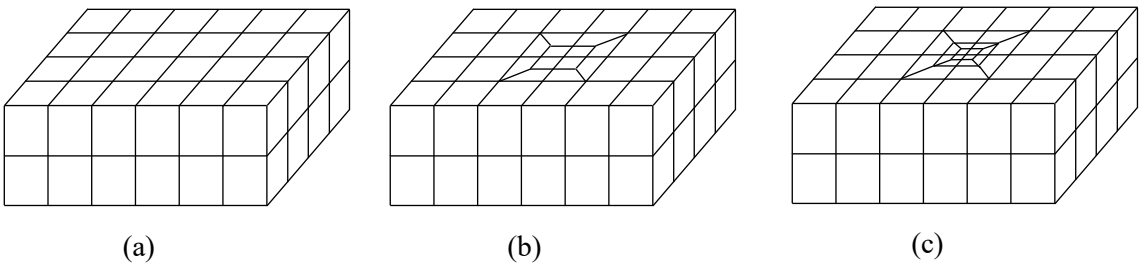

Fig. 4. Refinement of hexahedral mesh at a point on surface, a) initial element mesh, b) first refinement, c) second refinement

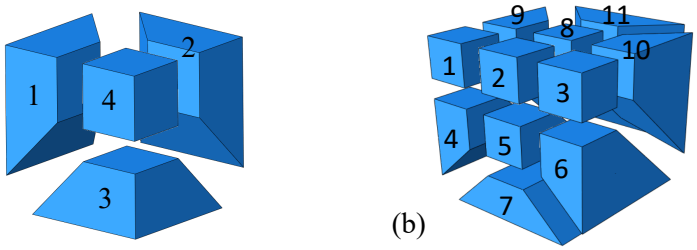

Fig. 5. Elements formed in a divided element for a) 4-element, b) 11-element

3. Analysis

Three specific examples were analyzed: the cubic block loaded with a single point loading, the rectangular block with shear loading, and the rectangular block containing a circular hole under uniform tension loading. Analyses were made by writing a code in MATLAB. In order to perform adaptive finite element analysis, an initial finite element analysis is made using an initial mesh. Then the mesh refinement is done using the stresses obtained. The final results are obtained by finite element analysis using the refined mesh.

In addition, the results were compared with the results obtained from ABAQUS finite element software, which is frequently used in the literature.

3.1. Material properties

In the analyses, material constants C_{10} and C_{01} for the Mooney-Rivlin material model were taken as 0,552 MPa and 0,138 MPa, respectively. Within the small strain range, the shear modulus, G, of the material is equal to $2(C_{10}+C_{01})$, and it can be calculated as 1,38 MPa and the elasticity modulus, E, can be calculated as 4,14 MPa. Poisson's ratio can be calculated by the following equation.

$$\nu=\frac{\frac{3K}{2G}-1}{3\frac{K}{G}+1} \tag{18}$$

The bulk modulus is taken as 1000 MPa. The Poisson's ratio values calculated for different bulk moduli are given in Table 2. In the penalty method, a high K value causes an instability called "volumetric locking". A small change in displacement value leads to a large change in pressure due to the large K value. For this reason, the finite element exhibits a more rigid behavior and changes shape less. For nearly incompressible materials, it will be sufficient to use a K value that produces a Poisson's ratio close to 0.5.

Table 2. Poisson's ratio corresponding to certain bulk modulus values for C_{10} = 0,552 and C_{01}=0,138

K (MPa)	*v*
1	0,0274
3	0,3006
5	0,3736
10	0,4340
100	0,4931
1000	0,4993
10000	0,4999

3.2. Single point loading on a cubic block

The cubic block has a side length of 100 mm. Displacements of the bottom surface points are constrained as shown in Fig. 6a. Single point pressure loading was applied on mid point of the upper face of the block. Analyzes were made using adaptive mesh refinement. Initial mesh of the adaptive refinement has 216 uniformly distributed hexahedral elements as shown in Fig. 7a. Normal stress, σ_{22}, in the direction of the point load was used as the effective stress parameter for adaptive mesh refinement criterion. Two successive adaptive analyzes were made. Finite element meshes after two adaptive refinements are shown in Fig. 7b and 7c.

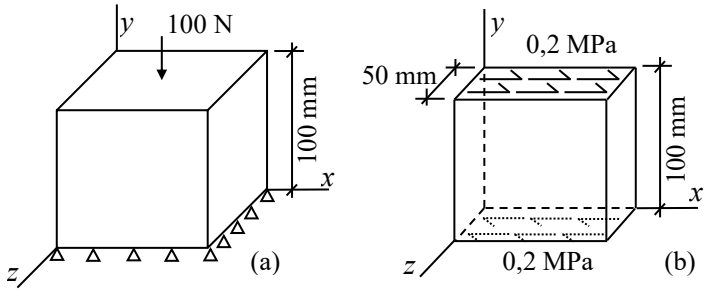

Fig. 6. a) Single point loading and b) shear loading applied on rectangular block

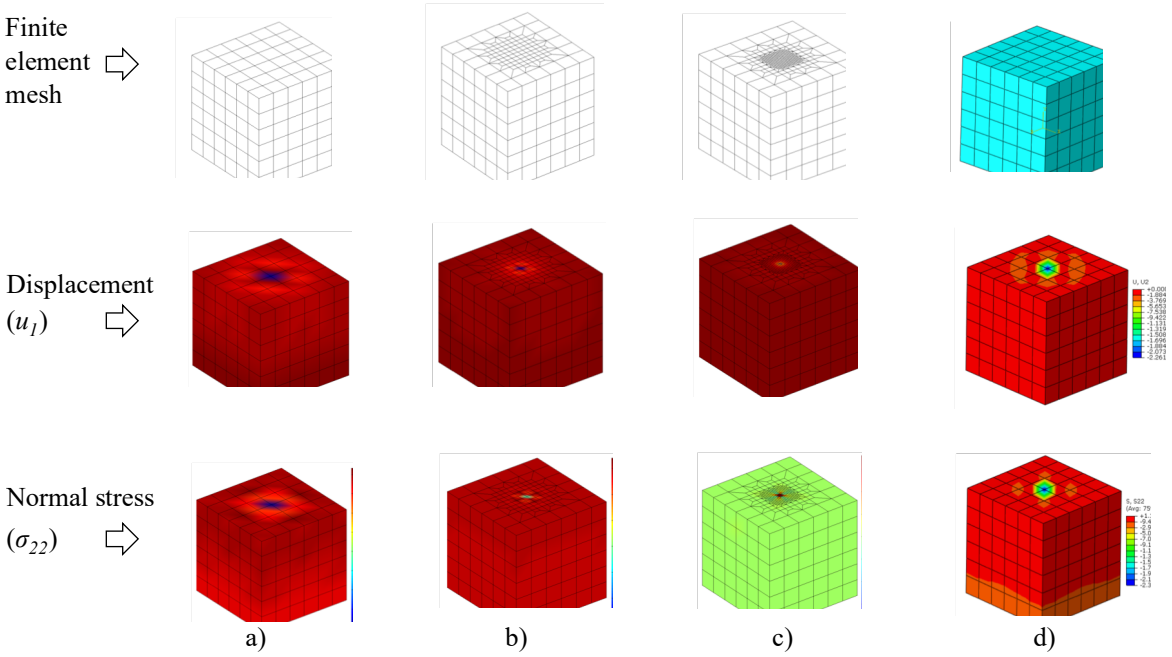

Fig. 7. a) initial mesh, b) first adaptive mesh refinement, c) second adaptive mesh refinement

The maximum displacement in y-direction, $u_{2_{max}}$, and maximum normal stress in y-direction, $\sigma_{22_{max}}$, are shown in Table 3. After the second adaptive analysis, the number of elements increases to 3108 elements, and the minimum element edge length decreases to 1,85, that is 11% of the minimum element edge length of the initial mesh.

The maximum displacement in the y-direction occurs at the point of application of the force. Its value varies between 2,18 mm and 7,63 mm as the number of elements increases for adaptive finite element analysis. The maximum normal stress occurs at the point of application of the

force. It varies between 0,164 MPa and 0,811 MPa as the number of elements increases for adaptive finite element analysis.

Table 3. Maximum u_2 displacement and maximum σ_{22} stress for adaptive mesh refinement

Analysis name	Number of elements	Minimum element edge length (mm)	$u_{2_{max}}$ (mm)	$\sigma_{22_{max}}$ (MPa)
Initial mesh analysis	216	16,7	2,18	0,164
First adaptive analysis	1016	5,55	6,17	0,791
Second adaptive analysis	3108	1,85	8,05	0,811

In addition, analyzes were also made using uniform mesh refinement where all the elements in the mesh were divided. Maximum displacement in *y*-direction and corresponding maximum normal stress obtained after four consecutive analyzes, are shown in Table 4. After the 4th uniform mesh refinement, the number of elements increases to 2744 elements, and the minimum element edge length decreases to 7,14, that is 43% of the minimum element edge length of the initial mesh.

Table 4. Maximum u_2 displacement and maximum σ_{22} stress for uniform mesh refinement

Analysis #	Number of elements	Minimum element edge length (mm)	$u_{2_{max}}$ (mm)	$u_{2_{max}}$ (mm) (Abaqus)	Difference (%)	$\sigma_{22_{max}}$ (MPa)	$\sigma_{22_{max}}$ (MPa) (Abaqus)	Difference (%)
1	216	16,7	2,18	2,26	3,54	0,164	0,234	29,91
2	512	12,5	2,86	2,96	3,38	0,265	0,373	28,95
3	1000	10	3,52	3,6	2,22	0,364	0,497	26,76
4	2744	7,14	4,76	4,89	2,66	0,538	0,892	39,69

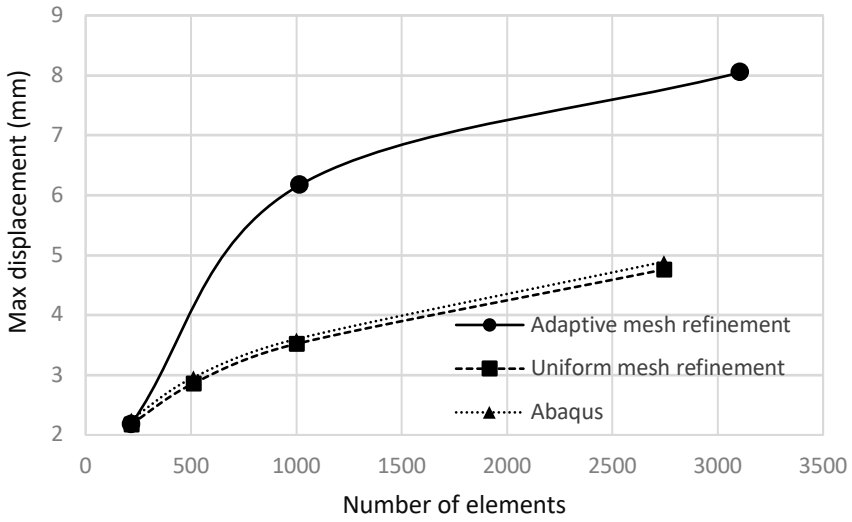

Fig. 8. Variation of maximum displacement $u_{2_{max}}$ with the number of elements

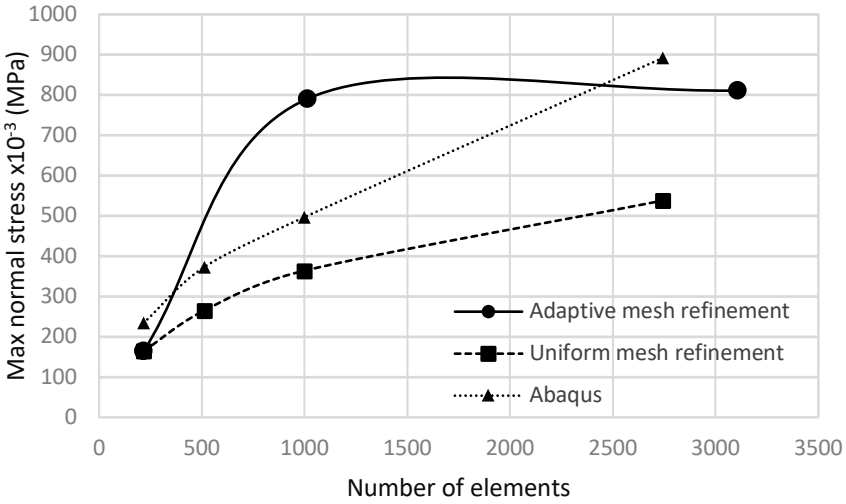

Fig. 9. Variation of maximum normal stress $\sigma_{22_{max}}$ with number of elements

In uniform mesh refinement, maximum displacement in the *y*-direction varies between 2,18 mm and 4,76 mm. The % difference between the results of uniform mesh refinement and Abaqus decreases as the number of elements increases.

Fig. 8 and Fig. 9 show the variation of maximum displacement, $u_{2_{max}}$, and variation of the maximum normal stress, $\sigma_{22_{max}}$, with the number of elements. These graphs represent convergence when adaptive mesh refinement was used.

3.3. Shear loading from the top surface on a rectangular block

The rectangular block, shown in Fig. 6b, is loaded at the bottom and top surface with a tangential surface traction of 0,2 MPa. Analyzes were made using two consecutive adaptive mesh refinements. Shear stress, σ_{12}, was used as the effective stress parameter for adaptive mesh refinement criterion. The number of elements created is given in Table 5. Maximum displacement in the x-direction, $u_{1_{max}}$, was calculated near the top and bottom edge of the problem geometry in the force direction. The maximum value of shear stress, $\sigma_{12_{max}}$, was obtained in the mid region of the problem geometry. The variation of maximum displacement in the x-direction, $u_{1_{max}}$, and variation of maximum shear stresses, $\sigma_{12_{max}}$, with the number of elements are shown in Fig. 10 and Fig. 11, respectively. Adaptive analysis converged after the first adaptive mesh refinement.

Table 5. Maximum u_1 displacement and maximum shear σ_{12} stress for adaptive mesh refinement

Analysis name	Number of elements	Minimum element edge length (mm)	$u_{1_{max}}$ (mm)	$\sigma_{12_{max}}$ (MPa)
Initial mesh analysis	108	16,7	9,73	0,265
First adaptive analysis	1542	5,55	10,12	0,277
Second adaptive analysis	10920	1,85	10,14	0,279

Analyzes were also performed using five uniform meshes by increasing the number of elements, as shown in Table 6. The problem was also analyzed using the Abaqus software with identical mesh distributions. Code written in MATLAB and Abaqus software yields similar results for

uniform mesh refinement. The maximum displacement value, $u_{1_{max}}$, and maximum shear stress, $\sigma_{12_{max}}$, for uniform mesh refinement apparently converged as the number of elements increased.

Table 6. Maximum u_1 displacement and maximum σ_{12} stress values for various uniform mesh refinements

Analysis #	Number of elements	Minimum element edge length (mm)	$u_{1_{max}}$ (mm)	$u_{1_{max}}$ (mm) (Abaqus)	Difference (%)	$\sigma_{12_{max}}$ (MPa)	$\sigma_{12_{max}}$ (MPa) (Abaqus)	Difference (%)
1	108	16,7	9,73	10,31	5,63	0,265	0,283	6,36
2	256	12,5	10,18	10,39	2,02	0,279	0,289	3,46
3	500	10	10,31	10,47	1,53	0,286	0,292	2,05
4	864	8,33	10,40	10,50	0,95	0,290	0,293	1,02
5	4000	5	10,52	10,60	0,75	0,294	0,297	1,01

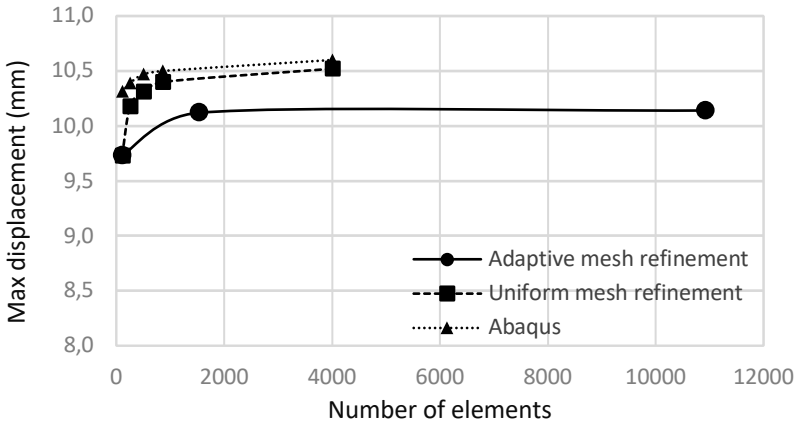

Fig. 10. Variation of maximum displacement $u_{1_{max}}$ with number of elements

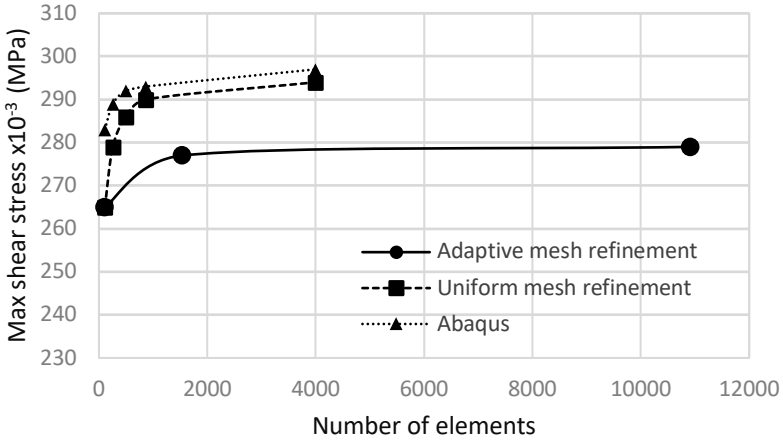

Fig. 11. Variation of maximum shear stress $\sigma_{12_{max}}$ with number of elements

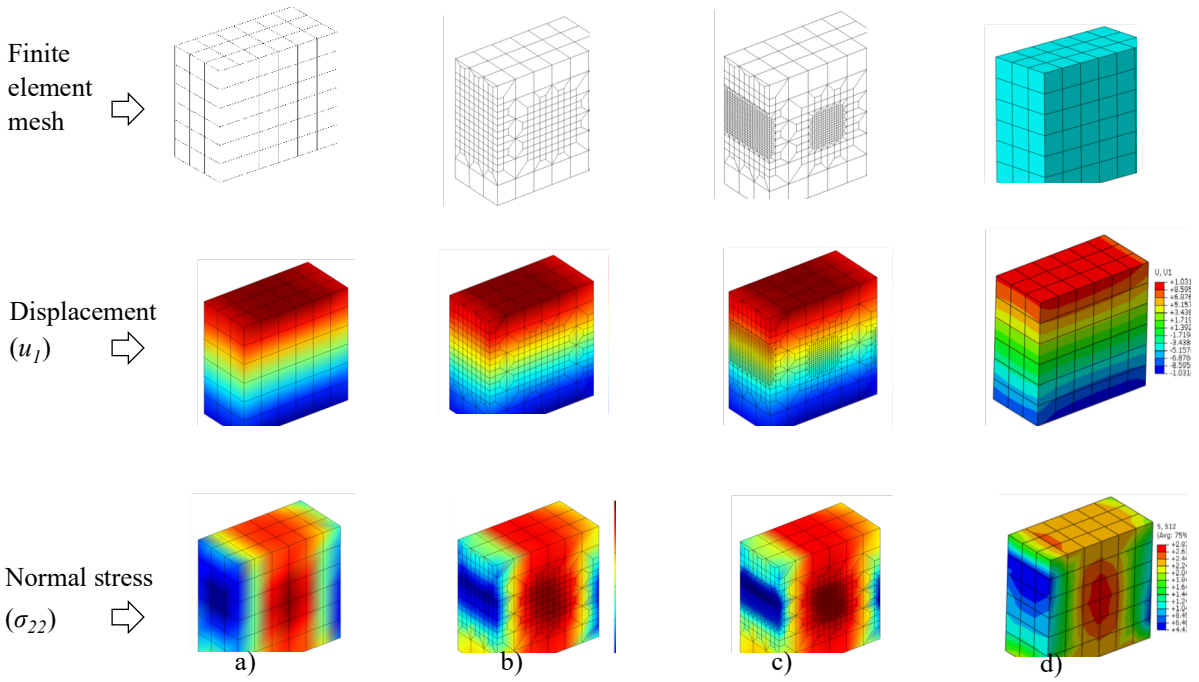

Fig. 12. Variation of displacement (u_1) and shear stress (σ_{12}) obtained from a) initial mesh, b) first adaptive mesh, c) second adaptive mesh, d) Abaqus

3.4. Rectangular block with circular hole

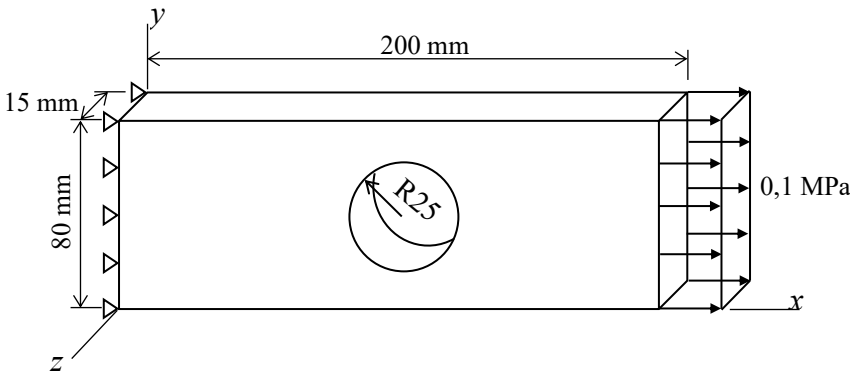

Fig. 13. Problem geometry, boundary conditions and applied force

Among the problems involving geometric discontinuities, the most frequently used problem geometry is a continuous medium containing a circular hole. Dimension of such a geometriy is given in Fig. 13. The nodes on left end of the rectangular block is restrained not to move along the x-direction and a distributed load is applied on the right end as the boundary conditions.
After the initial finite element mesh was created using 600 elements, two consecutive adaptive analyzes were carried. Normal stress, σ_{11}, in the direction of the tension load was used as the effective stress parameter for adaptive mesh refinement criterion. In Table 7, the maximum values of displacement in the x-direction and maximum normal stress obtained from these adaptive analyzes are presented. Also, the variation of displacements and shear stresses are shown in Fig. 14.

Table 7. Maximum u_1 displacement and maximum σ_{11} stress obtained from adaptive mesh refinement

Analysis name	Number of elements	Smallest element edge length (mm)	$u_{1_{max}}$ (mm)	$\sigma_{11_{max}}$ (MPa)
Initial mesh analysis	600	6,54	7,61	0,435
First adaptive analysis	2230	2,18	7,81	0,509
Second adaptive analysis	11770	0,73	7,81	0,594

Maximum normal stresses $\sigma_{11_{max}}$ were observed at the lower and upper midpoints of the circular hole. Maximum displacements $u_{1_{max}}$ were observed at the midpoint of the upper and lower edges of the surface to which the load is applied.

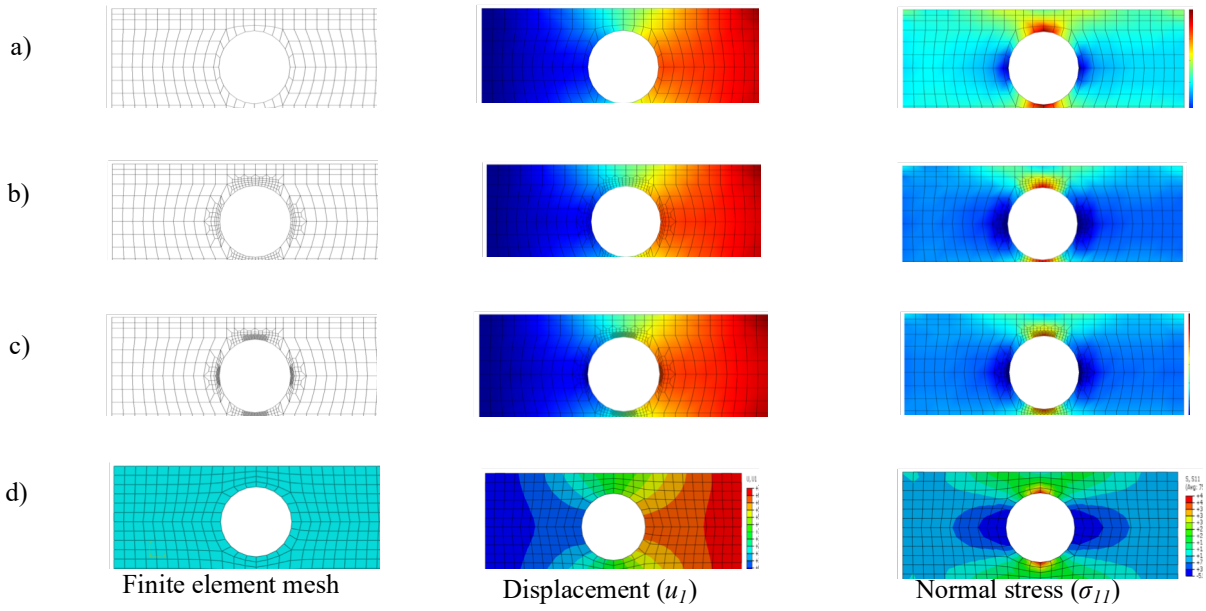

Fig. 14. Variation of displacement (u_1) and normal stress (σ_{11}) obtained from a) initial mesh, b) first adaptive mesh, c) second adaptive mesh, d) Abaqus

Analysis also was carried out for five separate uniform finite element meshes. The results for the maximum displacement, $u_{1_{max}}$, and maximum normal stress, $\sigma_{11_{max}}$, obtained using these meshes are shown in Table 8 in comparison with the results of Abaqus.

Fig. 14 and Fig. 15 show that the displacements were converged for the adaptive mesh analysis, and the normal stresses almost converged after second refinement. It has been also observed that the code written in MATLAB and Abaqus yield convergent solutions for the displacements and normal stresses in uniform distributions.

Table 8. Maximum u_1 displacement and maximum σ_{11} stress

Analysis #	Number of elements	Smallest element edge length (mm)	$u_{1_{max}}$ (mm)	$u_{1_{max}}$ (mm) (Abaqus)	Difference (%)	$\sigma_{11_{max}}$ (MPa)	$\sigma_{11_{max}}$ (MPa) (Abaqus)	Difference (%)
1	600	6,54	7,61	7,5	-1,47	0,435	0,480	9,38
2	1332	4,91	7,63	7,57	-0,79	0,442	0,487	9,24
3	1932	3,93	7,65	7,61	-0,53	0,450	0,491	8,35
4	3360	3,27	7,65	7,62	-0,39	0,464	0,497	6,64
5	4260	2,8	7,66	7,63	-0,39	0,465	0,499	6,81

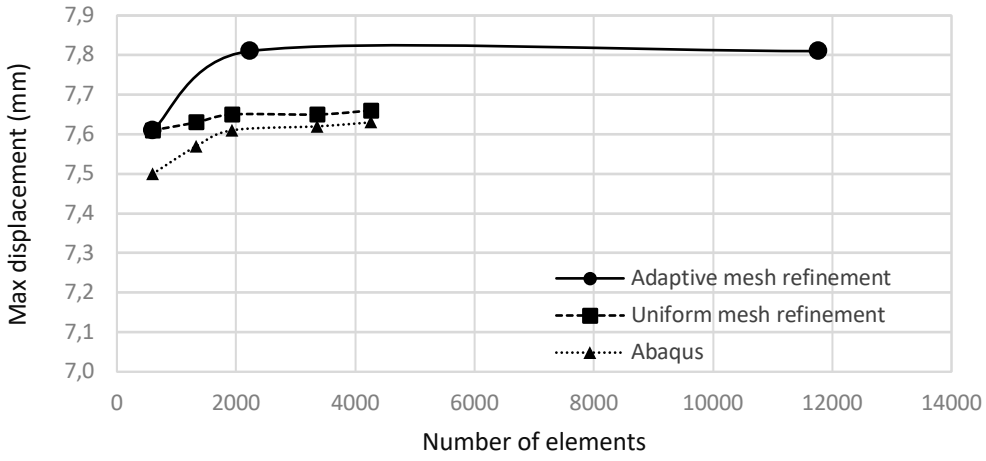

Fig.14. Variation of maximum displacement $u_{1_{max}}$ with number of elements

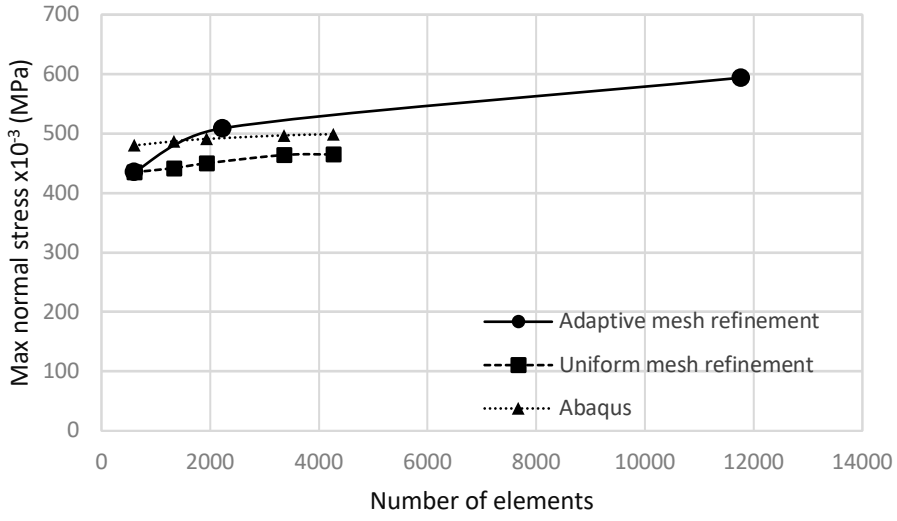

Fig.15. Variation of maximum normal stress $\sigma_{11_{max}}$ with number of elements

4. Conclusions

In this study, considering the large deformation of hyperelastic continuum, displacement and stress calculations were made using the Mooney-Rivlin material model and adaptive finite element analysis with hexahedral elements. Although there are sufficient studies on creating adaptive mesh using hexahedral elements, new studies are needed on its use for large deformation calculations with the finite element method. In this regard, a code has been written in the MATLAB environment. In order to check the reliability of the code, the test problems with the uniform mesh distributions were also solved with the Abaqus software. Comparisons show that the code written in MATLAB and Abaqus yields compatible results. Adaptive mesh refinement of hexahedral elements in the finite element analysis was performed using transition elements.

For the example of single point loading on a cubic block, the smallest element edge length decreased by approximately 90 percent in the adaptive finite element mesh, and the maximum displacement (u_2) and maximum normal stress (σ_{22}) values converged after the first adaptive solution. In the uniform mesh, the smallest element edge length decreased by approximately 60 percent. Maximum displacement (u_2) and maximum normal stress (σ_{22}) values converged faster than the adaptive finite element results. The maximum normal stress (σ_{22}) value obtained from the adaptive solution is approximately 10 percent less than the Abaqus solution.

For the shear loading from the top and bottom surfaces, the smallest element edge length decreased by approximately 90 percent in the adaptive mesh. The maximum displacement (u_1) and maximum shear stress (σ_{12}) values converged after the first adaptive solution. In the uniform mesh, the smallest element edge length decreased by approximately 70 percent. The maximum displacement (u_1) and maximum shear stress (σ_{12}) values converged for both the adaptive mesh refinement and the uniform mesh. The adaptive solution maximum shear stress (σ_{12}) value is approximately 6 percent less than the Abaqus.

For the rectangular block with a circular hole, the smallest element edge length around the circle decreased by approximately 90 percent in the adaptive mesh refinement. The maximum displacement (u_1) values converged after the first adaptive solution. The smallest element edge length decreased by approximately 60 percent in the uniform mesh. The maximum displacement value converged to 7,8mm after the first adaptive refinement. The maximum normal stress (σ_{11}) value almost converged for the uniform mesh. The difference between the results of the adaptive finite element solution and uniform mesh solution is approximately 16 percent for the maximum normal stress (σ_{11}) value.

The displacements obtained from the finite element solutions are large; for example, the displacements were between 4% and 11% of the problem geometry.

In order to create a uniform mesh distribution with the smallest element size as in the adaptive mesh refinement, many more elements need to be used. In this case, the solution time increases. Thus, adaptive distribution provides an advantage by shortening the solution time.
It can be seen that the criterion used in adaptive mesh refinement effectively creates locally refined elements.

For local mesh refinements, the transition from large to small elements must be smooth. In the case of hexahedral elements, the use of transition elements causes the formation of sharp internal angle elements in the transition from the larger to the smaller elements. In this case, the element mesh is not smooth enough. Considering the effect of this situation on the results, a smoothing procedure can be recommended to improve the results.

More realistic simulations can be made for tearing/rupture due to large deformations of the hyperelastic continuum by using adaptive mesh refinement with hexahedral elements.

References

[1] Blacker, T., Automated conformal hexahedral meshing constraints, challenges and opportunities. *Engineering with Computers,* 17, 201-210, 2002.

[2] Tadepalli, S.C., Erdemir, A. and Cavanagh, P.R., Comparison of hexahedral and tetrahedral elements in finite element analysis of the foot and footwear. *Journal of Biomechanics,* 44, 2337-2343, 2011.

[3] Schneiders, R., A grid-based algorithm for the generation of hexahedral element meshes. *Engineering with Computers,* 12, 168-177, 1996.

[4] Eppstein, E., Linear complexity hexahedral mesh generation. *Computational Geometry Theory and Applications,* 12, 3-16, 1999.

[5] Baudouin, T.C., Remacle, J.F., Marchandise, E., Henrotte, F. and Geuzaine, C., A frontal approach to hex-dominant mesh generation. *Advanced Modeling and Simulation in Engineering Sciences*, 1-8,2014.

[6] Staten, M.L., Canann, S.A. and Owen, S.J., *BMSweep: Locating interior nodes during sweeping. Engineering with Computers,* 15, 212-218, 1999.

[7] Lai, M., Benzley, S. and White, D., Automated hexahedral mesh generation by generalized multiple source to multiple target sweeping. *International Journal for Numerical Methods in Engineering,* 49, 261-275, 2000.

[8] Owen, S.J. and Saigal, S., H-Morph: an indirect approach to advancing front hex meshing. *International Journal for Numerical Methods in Engineering,* 49, 289-312, 2000.

[9] Li, T.S., McKeag, R.M. and Armstrong, C.G., Hexahedral meshing using midpoint subdivision and integer programming. *Computer Methods in Applied Mechanics and Engineering,* 124, 171-193, 1995.

[10] Schneiders, R., Refining quadrilateral and hexahedral element meshes, *Proceedings of the Fifth International Conference on Numerical Grid Generation in Computational Field Simulations,* 679-688, 1996.

[11] Harris, N.J., Benzley, S.E. and Owen, S.J., Conformal refinement of all-hexahedral element meshes based on multiple twist plane insertion, *Proceedings of the 13th International Meshing Roundtable (IMR),* 157–168, 2004.

[12] Parrish, M., Borden, M., Staten, M. and Benzley, S., A selective approach to conformal

refinement of unstructured hexahedral finite element meshes, *Proceedings of the 16th International Meshing Roundtable (IMR),* Seattle, USA, 14-17 Oct 2007.

[13] Huang, L., Zhao, G., Wang, Z. and Zhang, X., Adaptive hexahedral mesh generation and regeneration using an improve d grid-base d method. *Advances in Engineering Software,* 102, 49-70, 2016.

[14] Huang, L., Zhao, G., Ma, X. and Wang, Z., Incorporating improved refinement techniques for a grid-based geometrically-adaptive hexahedral mesh generation algorithm. *Advances in Engineering Software,* 64, 20-32, 2013.

[15] Tchon, K.F., Khachan, M., Guibault, F. and Camarero, R., Three-dimensional anisotropic geometric metrics based on local domain curvature and thickness. *Computer-Aided Design,* 37, 173-187, 2005.

[16] Zhang, Y. and Bajaj, C., Adaptive and quality quadrilateral/hexahedral meshing from volumetric data. *Computer Methods Applied Mechanics and Engineering,* 195, 942–960, 2006.

[17] Fernandes, J.L.M. and Martins, P.A.F., All-hexahedral remeshing for the finite element analysis of metal forming processes. *Finite Elements in Analysis and Design,* 43, 666 – 679, 2007.

[18] Zhao, G., Zhang, H. and Cheng, L., Geometry-adaptive generation algorithm and boundary match method for initial hexahedral element mesh. *Engineering with Computers,* 24, 321–339, 2008.

[19] Sun, L., Zhao, G. and Ma, X., Adaptive generation and local refinement methods of three-dimensional hexahedral element mesh. *Finite Elements in Analysis and Design,* 50, 184–200, 2012.

[20] Zhu, J. and Zienkiewicz, C., Super convergence recovery technique and a posteriori error estimators. *International Journal for Numerical Methods in Engineering,* 30, 1321-1339, 1990.

[21] Devloo, P. R., A three-dimensional adaptive finite element strategy. *Computers and Structures,* 38, 121-130, 1991.

[22] Zienkiewicz, O.C. and Zhu, J.Z., The superconvergent patch recover (SPR) and adaptive finite element refinement. *Computer Methods in Applied Mechanics and Engineering,* 101, 207-224, 1992.

[23] Wada, Y. and Okuda, H., *Effective adaptation technique for hexahedral mesh. Concurrency and Computation: Practice And Experience,* 14, 451-463, 2002.

[24] Park, C.,H. and Yang, D.Y., Adaptive refinement of all-hexahedral elements for three-dimensional metal forming analysis. *Finite Elements in Analysis and Design,* 43, 22–35, 2006.

[25] Moshfegh, R., Li, X. and Nilsson, L., Gradient-based refinement indicators in adaptive finite element analysis with special reference to sheet metal forming. *Engineering Computations,* 17, 910-932, 2000.

[26] Niekamp, R. and Stein, E., An object-oriented approach for parallel two- and three-dimensional adaptive finite element computations. *Computers and Structures,* 80, 317–328, 2002.

[27] Swanson, S. R., Large deformation finite element calculations for slightly compressible hyperelastic materials. *Computers and Structures,* 21, 81-88, 1985.

[28] Pengt, S. H. and Cbang, W. V., A compressible approach in finite element analysis of rubber-elastic materials. *Computers and Structures,* 62, 573-593, 1997.

[29] Suchocki, C., Finite element implementation of slightly compressible and incompressible first invariant-based hyperelasticity: theory, coding, exemplary problems. *Journal of Theoretical and Applied Mechanics,* 55, 787-800, 2017.

[30] Herrmann, L. R., Elasticity equations for incompressible and nearly incompressible materials by a variational theorem. *American Institute of Aeronautics and Astronautics (AIAA) Journal,* 3, 1896-1900, 1965.

[31] Bonet, J. and Bhargava, P., A uniform deformation gradient hexahedron element with artificial hourglass control. *International Journal For Numerical Methods in Engineering,* 38, 2809-2828, 1995.

[32] Neto, E. A. S., Peril D., Dutko M. and Owen D. R. J., Design of simple low order finite elements for large strain analysis of nearly incompressible solids. *International Journal of Solids and Structures,* 33, 3211-3296, 1996.

[33] Pascon, J. P., Large deformation analysis of plane-stress hyperelastic problems via triangular membrane finite elements. *International Journal of Advanced Structural Engineering,* 11, 331–350, 2019.

[34] Medri, G. and Strozzl, A., Mechanical analysis of elastomeric seals by numerical methods. *Industrial and Engineering Chemistry Product Research and Development,* 23, 596-600, 1984.

[35] Kato, K., Lee, N.S. and Bathe K.J., Adaptive finite element analysis of large strain elastic response. *Computers and Structures,* 47, 829-855, 1993.

[36] Chamberland, E., Fortin, A. and Fortin, M., Comparison of the performance of some finite element discretizations for large deformation elasticity problems. *Computers and Structures,* 88, 664–673, 2010.

[37] O'Shea, D. J., Attard, M. M., Kellermann, D.C. and Sansour, C., Nonlinear finite element formulation based on invariant-free hyperelasticity for orthotropic materials. *International Journal of Solids and Structures,* 185, 191-201, 2000.

[38] Nguyen, T. D., Huynh, T. T. H., Nguyen, N. T., Nguyen, H. T. M. and Truong, T. T., Finite element analysis for three-dimensional hyper-elastic problems. *Science and Technology Development Journal,* 24, 43-50, 2022.

[39] Schönherr, J. A., Schneider, P. and Mittelstedt, C., Robust hybrid/mixed finite elements for rubber-likematerials under. *Computational Mechanics,* 70, 101–122, 2022.

[40] Onishi, Y. and Amaya, K., A locking-free selective smoothed finite element method using tetrahedral and triangular elements with adaptive mesh rezoning for large deformation problems. *International Journal for Numerical Methods in Engineering,* 99, 354-371, 2014.

[41] Léger, S., Fortin, A., Tibirna, C. and Fortin, M., An updated Lagrangian method with error estimation and adaptive remeshing for very large deformation elasticity problems. *International Journal For Numerical Methods in Engineering,* 100, 1006–1030, 2014.

[42] Ju, X., Mahnken, R., Xu, Y. and Liang, L., Goal-oriented error estimation and h-adaptive finite elements for hyperelastic micromorphic continua. *Computational Mechanics,* 69, 847-863, 2022.

[43] Jansaria, C., Natarajana, S., Beexb, L. and Kannana, K., Goal-oriented error estimation and h-adaptive finite elements for hyperelastic micromorphic continua. *Computational Mechanics,* 69, 847–863, 2022.

[44] Meyer, A., Error estimators and the adaptive finite element method on large strain deformation problems. *Mathematical Methods in the Applied Sciences,* 32, 2148-2159, 2009.

[45] Léger, S. and Pepin, A., An updated Lagrangian method with error estimation and adaptive remeshing for very large deformation elasticity problems: The three-dimensional case. *Computer Methods Applied Mechanics and Engineering,* 309, 1–18, 2016.

[46] Smith, M., *ABAQUS/Standard User's Manual*, Version 6.9, Dassault Systemes, Simulia Corp, 2009.

[47] Kim, N.H., *Introduction to Nonlinear Finite Element Analysis,* Springer, 2015.

[48] Shabana, A.A. and Niamathullah, S.K., Total Lagrangian Formulation For Large-Displacement Analysis Of The Triangular Finite Elements. *Computer Methods in Applied Mechanics And Engineering,* 72, 195-199, 1989.

[49] Wriggers, P., *Nonlinear Finite Element Methods*, Springer, 2008.

[50] Zienkiewicz, O.C., Zhu, J.Z. and Gong, N.G., Effective and Practical h–p Adaptive Analysis Procedure for the Finite Element Method, *International Journal for Numerical Methods in Engineering,* 28, 879-891, 1989.